Food Chemistry: X 18 (2023) 100675

Contents lists available at ScienceDirect

Food Chemistry: X

journal homepage: www.sciencedirect.com/journal/food-chemistry-x

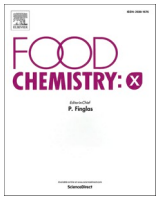

Effect of honeysuckle leaf extract on the physicochemical properties of carboxymethyl konjac glucomannan/konjac glucomannan/gelatin composite edible film

Meng Wang [a,1], Yun-Cheng Li [a,b,1], Fan-Bing Meng [a,b,*], Qiao Wang [c], Zheng-Wu Wang [b], Da-Yu Liu [a]

[a] College of Food and Biological Engineering, Chengdu University, Chengdu 610106, PR China
[b] Shanghai Jiao Tong University Sichuan Research Institute, Chengdu 610218, PR China
[c] Sichuan Institute of Food Inspection, Chengdu 610097, PR China

ARTICLE INFO

Keywords:
Bioactive edible film
Carboxymethyl konjac glucomannan
Gelatin
Honeysuckle leaf extract

ABSTRACT

Honeysuckle leaves are rich in bioactive ingredients, but often considered as agro-wastes. In this study, honeysuckle leaf extract (HLE) was added to the carboxymethyl konjac glucomannan/konjac glucomannan/gelatin composite edible film (CMKH). Compared to films without HLE addition (CMK), the water vapor barrier properties of CMKH slightly decreased, but the transmittance of the CMKH films in UV region (200–400 nm) as low as zero. The elongation at break of CMKH film was 1.39 ~ 1.5 fold higher than those of CMK films. The DPPH and ABTS scavenging activity of CMKH-II was 85.75% and 90.93%, respectively, which is similar to the equivalent content of Vc. The inhibition rate of CMKH-I and CMKH-II against *Escherichia coli* and *Listeria monocytogenes* were close to 90%, and the inhibition rate against *Staphylococcus aureus* were up to 96%. The results emphasized that the composite film containing 25% (v/v) HLE has potential application value in food preservation.

1. Introduction

Food packaging can help to extend the shelf life of foods. Currently, food packaging materials are mainly petroleum-based plastic packaging (Lei et al., 2019), which is also called “white pollution”. Wide application of plastic packaging can cause environmental damage, leading to prominent health concerns. Therefore, there is now great interest in developing active packaging using natural polymers (Biao et al., 2019). Active packaging is one of the most promising packaging technologies that can not only extend shelf life but also improve safety and sensory properties (Lei et al., 2019). In addition, the natural active ingredients used to prepare active packaging mainly come from plants or microorganisms, and these ingredients are often functional compounds in foods; thus, edible active packaging can also improve the nutritional quality of foods. Various natural polymers are used to prepare edible packaging films, including proteins, lipids, polysaccharides (Marangoni Júnior & Gonçalves, 2022). Among them, konjac glucomannan (KGM) has proven to be a promising candidate material because of its abundance, excellent film-forming ability, biodegradability, and bioavailability (Liu, Lin, Lopez-Sanchez, & Yang, 2020). However, natural KGM has strong hydrophilicity, but its hydrophobicity is insufficient, which limits its application in the encapsulation of bioactive ingredients; thus, hydrophobic modification is usually performed (Meng, Gou, et al., 2022). Carboxymethyl konjac glucomannan (CMKGM) is one of the most important derivatives of KGM, and CMKGM is a typical anionic polysaccharide with amphiphilic properties due to carboxymethylation and deacetylation could endow its hydrophobicity (Xiao et al., 2015). CMKGM is often used in the preparation of nanogels (Wang, Zhou, Zheng, & Pang, 2022), but there are few studies on the preparation of active packaging films by CMKGM.

Films prepared from a single material have some limitations, such as poor chemophysical properties, unsuitable mechanical performance, or poor embedding ability for active ingredients, which restricts their applications in practical packaging (Lei et al., 2019). The preparation of bioactive edible films by blending various biopolymer materials is an efficient technique to enhance the properties of bioactive films. The blend film with better compatibility has better mechanical and barrier properties. In particular, polysaccharide and protein blend films are

* Corresponding author at: College of Food and Biological Engineering, Chengdu University, No. 2025 Chengluo Road, Chengdu, China.
E-mail address: mfb1020@126.com (F.-B. Meng).
[1] These authors contributed equally to this work.

https://doi.org/10.1016/j.fochx.2023.100675
Received 28 February 2023; Received in revised form 4 April 2023; Accepted 4 April 2023
Available online 8 April 2023

particularly significant in terms of performance improvement (Zhang, Zhu, et al. 2022). Gelatin, as a collagen hydrolysate, has good oxygen barrier properties and unique controlled release properties. Gelatin films exhibit excellent stretchability strength and excellent swelling in controlled release packaging technology. However, pure gelatin films also have many defects, such as high hydrophilicity and solubility (Rather et al., 2022). To date, gelatin has been combined with various polysaccharides to produce blended films with superior performance (Vargas-Torrico, von Borries-Medrano, & Aguilar-Mendez, 2022).

To increase the shelf life of food without potential risk, natural active ingredients are often introduced to packaging materials, such as antioxidants and antimicrobials (Marangoni Júnior & Gonçalves, 2022). Additionally, some active ingredients, such as natural polyphenols, could also enhance the physicochemical characteristics and functionality of edible films (Biao et al., 2019). Currently, natural active ingredients mainly extracted from plants or microorganisms. In China, honeysuckle (*Lonicera japonica* Thunb.) is a widely used edible and medicinal plant. Its flower buds are generally considered to be herb medicine and tea resource. The flowers are rich in active ingredients such as phenolics, terpenes, and organic acids, especially chlorogenic acid, which is a unique biologically active phenolic compound (Shang, Pan, Li, Miao, & Ding, 2011). During the production of honeysuckle flowers, the annual output of leaves is much larger than that of flower buds. Currently, most studies are aimed at the nutrition and function of honeysuckle flowers, and leaves are considered to be of low value and waste; thus, few studies on the utilization of honeysuckle leaves have been reported. However, recent studies have found that honeysuckle leaves show strong similarity in chemical composition with flower buds (Li, Kuang, Wang, Wan, & Li, 2020). If honeysuckle leaves can be used as resources, the economic benefits can be increased. Therefore, in this study, HLE was selected as the active substance to prepare bioactive edible film, and the effect of HLE on the properties and bioactivities (antibacterial and antioxidant activities) of the composite edible film was comprehensively evaluated. This work aimed to investigate the effect of HLE on the performance of biological edible films, create a new edible bioactive film, and to serve as a reference for the resource utilization of honeysuckle leaves.

2. Materials and methods

2.1. Bacterial strains and materials

Fresh honeysuckle leaves were collected from Chengdu Qinglonghu Park at 11:00 a.m. in early June. *Escherichia coli, Listeria monocytogenes,* and *Staphylococcus aureus* were purchased from Beijing Biobw Biotechnology Co. (Beijing, China). KGM (M_w = 2.895 × 10^6 g/mol, 95.0% purity) was supplied by the Anfu Konjac Development Co., Ltd (Mianyang, China). Gelatin (Type A, 250 Bloom, 40 mesh, dry-base protein content ≥ 98%, Mw = 1 ~ 7 × 10^4 g/mol) were obtained from Chengdu Cologne Chemical Co., Ltd. (Chengdu, China). Chlorogenic acid (purity 98%) was purchased from Shanghai Yuanye Bio-Technology Co., Ltd. (Shanghai, China). DPPH (2,2-diphenyl-1-picrylhydrazyl) was purchased from Sigma-Aldrich Chemical Co. (St. Louis, MO, USA). ABTS (2,2′-Azinobis (3-ethylbenzothiazoline-6-sulfonic acid ammonium salt) was purchased from Shanghai Hualan Chemical Technology Co., ltd. (Shanghai, China). Unless otherwise stated, all other compounds were of the analytical reagent grade.

2.2. Preparation of honeysuckle leaf extract (HLE)

The honeysuckle leaves were washed using tap water, air dried at 40 °C, and crushed. A total of 20 g of broken honeysuckle leaves was immersed in 100 mL of 50% ethanol and vigorously stirred at a speed of 100 r/min for 24 h at 37 °C. After filtration with a double layer of gauze, the liquid was centrifuged at 8000 × g for 15 min, the supernatant was vacuum-concentrated at 40 °C to a final volume of 40 mL, and HLE was obtained.

2.3. Preparation of CMKGM

KGM (5 g) was dispersed in 30 mL of 80% (v/v) ethanol, and then 3.34 g of chloroacetic acid was added to the system and stirred at 20 °C for 2 h. Twenty milliliter of 80% ethanol and 4.17 g of sodium hydroxide were added to the reaction system, and then magnetically stirred and heated at 55 °C for reacting 3 h. The reaction solution was then filtrated and first rinsed with 85% ethanol 3 times and then washed with absolute ethanol and filtrated. The filtrate was lastly dried at 60 °C, ground into powder and passed through a 100-mesh screen to obtain the product CMKGM, and the degree of substitution measured by potentiometric titration was 0.59.

2.4. Preparation of edible films

KGM, gelatin, CMKGM and glycerin were dissolved in 100 mL of ultrapure water according to the formula of Supplementary Table S1, magnetically stirred and heated at 55 °C until completely dissolved. After that the mixtures were centrifuged at 6000 × *g* for 5 min to remove insoluble impurities to make a uniform suspension. HLE was added to the suspension and evenly blended by magnetic stirring. Potassium sorbate (PS) was used for comparison. After centrifugation at 6000 × *g* for 3 min to eliminate air bubbles, the film-forming solution was allowed to stand for 2 h, poured into a polytetrafluoroethylene mold, and dried at 40 °C for 24 h. The film was taken out and put into a desiccator (relative humidity 53%, 25 °C) for further analysis. A film without CMKGM was designated KGL, and films with CMKGM were designated CMK-I and CMK-II. Films containing HLE were designated CMKH-I and CMKH-II, and films containing PS were designated CMKP-I and CMKP-II.

2.5. Evaluation of film-forming solutions

2.5.1. Particle size and zeta potential

The prepared film-forming solution was diluted at 1:100 with ultrapure water. According to the method of Meng et al. (2022), the particle size, polymer dispersity index (PDI) and zeta potential of the film-forming solution were measured using a laser particle size analyzer (ZEN3600, Malvern Instruments Ltd., UK) outfitted with a He-Ne laser (633 nm) and 90° collection optics at 25 °C.

2.5.2. Rheological measurement

Steady shear frequency sweeps measurements were performed using a CSL2 100 rheometer (Anton Paar, Germany) utilizing a measurement system with plate-plate geometry (50 mm diameter, 500 mm gap). Steady shear measurements were obtained at 25 °C. The flow curves were obtained by registering shear stress with increasing shear rates from 0.1 to 100 s^{-1}.

2.6. Detection of total phenolic content of films

The Folin-Ciocalteu method was used to determine the total phenolic content of CMKH films. A total of 50 mg of the film sample was smashed and dissolved in 10 mL of ultrapure water to make a film extract. Taking 1 mL of the extract and mixed with the Folin-Ciocalteu reagent (1:9 v/v) at ratio of 1:1 (v/v). After reacted 5 min at 30 °C, 2 mL of 20% Na_2CO_3 solution was added. After being placed in the dark at room temperature for 1 h, the absorbance of the mixture was measured at 760 nm with a Multiskan skyhigh1550 microplate reader (Thermo, USA). The total phenolic content was presented as milligrams of chlorogenic acid equivalent per unit gram of the film (mg CAE/g film).

2.7. Thickness, tensile strength (TS) and elongation at break (EB%) testing

The film thickness was measured with a digital micrometer (Sanliang Measuring Tool Co., Ltd., China), and the accurate value of the film thickness was 0.001 mm. The values for each film were calculated by the average of five different locations. All film samples were cut into 2 cm × 10 cm shapes, and the TS and EB% of the films were assessed at room temperature using a QL-5E electronic tensile tester (Xiamen Qunlong Instrument Co., Ltd., China) according to the recommended procedure of ASTM D882-88. The film samples were stretched at a speed of 500 mm/min under a tensile force (10 N) with an initial clamp length of 5 cm.

2.8. Film solubility and water vapor permeability (WVP)

Films (100 mg) were placed into a 50 mL centrifuge tube along with 20 mL of water. After being left at room temperature for 24 h, the mixture was centrifuged at 8000 × *g* for 15 min. After removing the supernatant, the precipitate was dried at 60 °C. Film solubility was expressed as weight loss (WL) calculated by the following Eqn.

$$WL\ (\%) = \left(\frac{Weight\ loss}{Initial\ weight}\right) \times 100$$

WVP was measured according to the description of Semwal, Ambatipudi, and Navani (2022) with slight modifications: 2 g of anhydrous $CaCl_2$ was added into a 40 mm × 25 mm weighing bottle and then covered with a sample film. The samples were placed in a chamber that maintained a constant temperature and relative humidity of 25 °C and 75%, respectively. The mass of the weighing bottle (with membrane) was recorded every hour until the mass reached a steady state. WVP was calculated using the following:

$$WVP = \frac{\Delta m}{\Delta P \times A \times \Delta t} \times d$$

where Δm represents the sample weight change (g), Δt represents the time interval (s), d represents the film thickness (m), A represents the effective area of the films (m^2), and ΔP represents the differential air pressure inside and outside of the films (Pa).

2.9. Light blocking properties and opacity

As described by Sáez-Orviz, Marcet, Rendueles, and Díaz (2021), the transmittance and absorption values were measured at various wavelengths between 200 and 800 nm using a UV-2600 spectrometer (Shimadzu, Japan) to study the light blocking properties, and opacity was calculated according to the following formula:

$$Opacity = \frac{A_{600}}{x}$$

where A_{600} is the absorbance of the film at 600 nm, and × is the film thickness (mm).

2.10. Chromatic aberration

The edible films were photographed using a 20-megapixel camera (D3200, Nikon, Japan). The chromatic aberration was measured according to Meng, Lei, et al. (2022) by using an NH300 colorimeter (Threenh Technology Co., Ltd., China). The values of CIE L^* (lightness), a^* (redness) and b^* (yellowness) were recorded by standardized with a white plate, and total color differences (ΔE) were calculated according to the following formula:

$$\Delta E = \sqrt{(L^* - L)^2 + (a^* - a)^2 + (b^* - b)^2}$$

2.11. Surface morphology analysis

2.11.1. Scanning electron microscopy (SEM) analysis

According to a previous study (Li et al., 2021), the surface morphology of the film was analyzed by using an SU 8020 scanning electron microscopy (SEM) device (Hitachi, Japan) Films were sputter-coated with gold under vacuum and scanned with a secondary electron detector operating at 20 KV.

2.11.2. Atomic force microscopy (AFM) analysis

The shapes of the films were observed by a Dimension Icon AFM instrument (Bruker, Germany). The scanning area of the film surface was 10 μm in width × 10 μm in length, and the scanning processes were performed at room temperature (25 °C). 3D imaging was performed using Gwyddion software.

2.12. X-ray diffraction (XRD)

An X-ray diffractometer (D8 ADVANCE, Bruker, Germany) with a Cu Kα radiation source (λ = 1.5406 Å) at 40 kV and 40 mA was used to perform XRD on the films. The scanning range of 2θ was 4-40° at a step size of 0.02°, count time of 2 s, and scanning speed of 2°/min.

2.13. Fourier transform infrared (FT-IR) spectroscopy

FT-IR spectra was obtained by an FT-IR spectroscopy instrument (Spectrum 3, Perkinelmer, USA) with record in the range of 4000–500 cm^{-1}, and the spectra were acquired at a resolution of 4 cm^{-1} and scanned 16 times (Zhang, Ma, Yang, Li, & Sun, 2022).

2.14. Thermogravimetric analysis

The thermal properties were investigated by a synchronous thermal analyzer (TGA/DSC 3+, Mettler, Switzerland). Ten milligrams of the samples were heated from 30 to 600 °C at a rate of 10 °C/min under a N_2 (purity ≥ 99.999%.) flow rate of 50 mL/min (Li et al., 2022)0.

2.15. Antioxidant activities analysis

2.15.1. DPPH radical scavenging activity of films

DPPH free radical scavenging activity was assessed in accordance with Rao et al. (2022). Dissolve 50 mg of the sample in 10 mL of ultrapure water to make a film extract. Then, mix 100 μL of the extract with 100 μL of 0.1 mmol/l DPPH ethanol solution in a 96-well plate, and kept at room temperature in dark for 30 min. The absorbance of the solutions was recorded at 517 nm by using a Multiskan skyhigh1550 microplate reader (Thermo).

2.15.2. ABTS radical scavenging activity

ABTS radical scavenging activity was assessed in accordance with Meng, Zhou, et al. (2022). A 7 mmol/L ABTS solution was prepared with 2.45 mmol/L potassium persulfate. The abovementioned solutions were mixed at a 1:1 ration and left at room temperature for 12 to 16 h in dark place. Dilute 1 mL of the mixture in 80 mL of ethanol, adjust the absorbance to 0.700 ~ 0.800 at 734 nm. Film extracts were prepared by dissolving 50 mg of the sample in 10 mL of distilled water. Then, 30 μL of the prepared sample was mixed with 170 μL of ABTS solution in a 96-well plate, the mixture was then reacted at 25 °C in dark place for 6 min. Absorbance was recorded at 734 nm by using a Synergy H1 microplate reader (BioTek, USA).

2.16. Antibacterial test

2.16.1. Disc diffusion method

The disc-diffusion method was assessed in accordance with Xue, Gu,

Wang, Li, and Adhikari (2019). The films were made into 15 mm-diameter discs, and irradiated by UV light for 20 min. The film discs were then placed on the surface of Luria-Bertani (LB) agar plates inoculated with 0.1 mL of inoculum containing indicator microorganisms (*E. coli, L. monocytogenes, and S. aureus*) in the concentration of 10^6 cfu/mL. The diameter of the inhibition zone around the film discs was recorded after the plates were incubated at 37 °C for 24 h.

2.16.2. Inhibition rate method

The antibacterial effects of the films were determined by the inhibition rate approach according to the description of He, Wang, Jiang, Liu, and Zhu (2021) with some changes. The films were divided into small pieces, and 100 mg of the pieces was added introduced to tubes with 5 mL of LB broth medium containing 10^6 cfu/mL indicator microorganisms. The samples were then cultured at 37 °C with gentle shaking for 6 h, after which the culture medium was taken and diluted and spread on LB agar plates to determine the number of viable bacteria and calculate the inhibition rate. The antibacterial test without films was served as a control, and the inhibition rate (%) was calculated according to the following formula:

$$Inhibitionrate(\%) = \frac{A - B}{A} \times 100\%$$

where A is the viable cells in blank plates, and B is the viable cells in film addition plates.

2.17. Statistical analysis

Statistical analysis was conducted by using SPSS software 20.0 (IBM Inc., USA). The results are expressed as the mean ± standard deviation (SD). Differences ($P < 0.05$) among means were evaluated by analysis of variance (ANOVA) with Duncan's test.

3. Results and discussion

3.1. Characteristics of film-forming solutions

3.1.1. Particle size, PDI and zeta potential (ZP)

A stable solution can form a film with a consistent thickness or surface permeability equilibrium upon drying. The low PDI value indicates homogeneous particles in the solution. As shown in Table 1, the particle size and PDI value of KGL are 0.98 μm and 0.76, respectively. After adding CMKGM, the particle sizes of CMK-I and CMK-II increased, but the PDI decreased, indicating that the addition of CMKGM helped uniformly disperse the film-forming solution. However, the addition of HLE and PS negatively affected the uniformity of the solution, but this influence was not significant.

ZP can reflect the film-forming solution stability. As shown in Table 1, the ZP of KGL was approximately −17.67 mV, and the ZP of the CMKP-I film-forming solution decreased to −20.63 mV. The ZP of the other film-forming solutions were between −37.7 mV and −56.71 mV. When the positive and negative potentials are greater than or less than + 30 mV and − 30 mV, respectively, the electrical particles in the solutions will repel each other, which is helpful for dispersion stability (Carneiro-da-Cunha, Cerqueira, Souza, Teixeira, & Vicente, 2011). Therefore, all film-forming solutions of CMK, CMKH, and CMKP have great stability.

3.1.2. Rheological behavior

Film-forming solutions with a moderate viscosity can help form uniform and even films (Shivangi, Dorairaj, Negi, & Shetty, 2021). As shown in Fig. 1A, all film-forming solutions at 25 °C exhibited a shear-thinning behavior, which was might because the unraveling and rearrangement of polymer chains under shear force. All solutions exhibited Herschel-Bulkley-type non-Newtonian behavior (Table 1). A significant reduction in viscosity was obtained at low shear rates, while at high shear rates, the viscosity change is low (Fig. 1A).

The addition of HLE reduced the viscosity of the film-forming solution. This may be because HLE are rich in various phenolic compounds, mainly chlorogenic acid. The total phenolic content (determined using chlorogenic acid as the standard) in the CMKH-I and CMKH-II films reached 37.00 and 38.68 mg CAE/g film, respectively (Table 1). The pH value of the HLE extract decreased due to the existence of natural phenolic acids, which further reduced the viscosity of the film-forming solution. In addition, the natural compounds in the HLE extracts could also weaken the interactions of the film-forming materials (Shivangi et al., 2021). The addition of PS can increase the viscosity of the film-forming solution.

3.2. Thickness, tensile strength (TS) and elongation at break (EB)

Film thickness could significantly impact on the light transmittance, WVP and mechanical strength. As shown in Table 2, the thickness of the CMK increased with increasing CMKGM content. The thickness of the film further increased with HLE and PS addition, but the thickness of the CMKP films was thicker than that of the CMKH film, probably due to the PS increasing the film porosity (Fidelis et al., 2022), which formed a spatial structure.

KGM and gelatin can provide good mechanical strength and toughness for the film, respectively. KGM can combine with the proteins in gelatin to form a winding network structure, so it has stronger interaction and extension strength (Ran, Lou, Zheng, Gu, & Yang, 2022). As shown in Table 2, the TS of KGL was 10.01 MPa, and the EB was 61%. The higher degree of deacetylation of KGM will result in stronger rigidity and stronger structure (Ran et al., 2022). So when adding 2% CMKGM, the EB of the CMK-I film increased to 81%. Although 3% CMKGM addition increased the TS of the CMK-II film, the EB decreased. After adding 2% HLE, the TS and EB of CMKH-I further increased to 113.15%, which is significantly greater than that of KGL edible films. This may be due to the addition of bioactive compounds create strong hydrogen bonds between functional groups such as hydroxyl, amino, and carboxymethyl groups; thus, the structure of CMKH-I became more compact (Shivangi et al., 2021). The TS of CMKH-II decreased, possibly

Table 1
Characteristics of film forming solutions.

Treatment	Particle size (μm)	PDI	Zeta potential (mV)	Rheological parameters			
				K	*n*	R	R^2
KGL	0.98 ± 0.14^{c}	0.75 ± 0.04	-17.67 ± 2.17^{a}	0.001 ± 0.0004^{e}	1.152 ± 0.068^{a}	0.985	0.970
CMK-I	1.24 ± 0.16^{c}	0.31 ± 0.01	-53.97 ± 2.44^{cd}	0.143 ± 0.012^{d}	0.971 ± 0.015^{b}	0.998	0.997
CMK-II	2.21 ± 0.15^{a}	0.39 ± 0.15	-39.98 ± 2.06^{b}	0.880 ± 0.056^{b}	0.835 ± 0.018^{c}	0.999	0.999
CMKH-I	1.15 ± 0.19^{c}	0.52 ± 0.02	-56.71 ± 1.40^{d}	0.091 ± 0.003^{d}	0.919 ± 0.010^{b}	0.999	0.999
CMKH-II	2.17 ± 0.10^{a}	0.47 ± 0.02	-48.27 ± 2.72^{c}	0.472 ± 0.008^{c}	0.834 ± 0.003^{c}	0.999	0.999
CMKP-I	1.51 ± 0.12^{b}	0.65 ± 0.04	-20.63 ± 2.17^{a}	0.133 ± 0.0004^{d}	0.954 ± 0.015^{b}	0.998	0.997
CMKP-II	1.98 ± 0.33^{a}	0.53 ± 0.02	-37.7 ± 2.26^{b}	0.978 ± 0.077^{a}	0.821 ± 0.019^{c}	0.999	0.998

K: consistency coefficient, *n*: flow behavior index, R and R^2: correlation coefficient. The value is mean ± standard deviation (n = 3). Different letters in the same column indicate significant difference ($p < 0.05$).

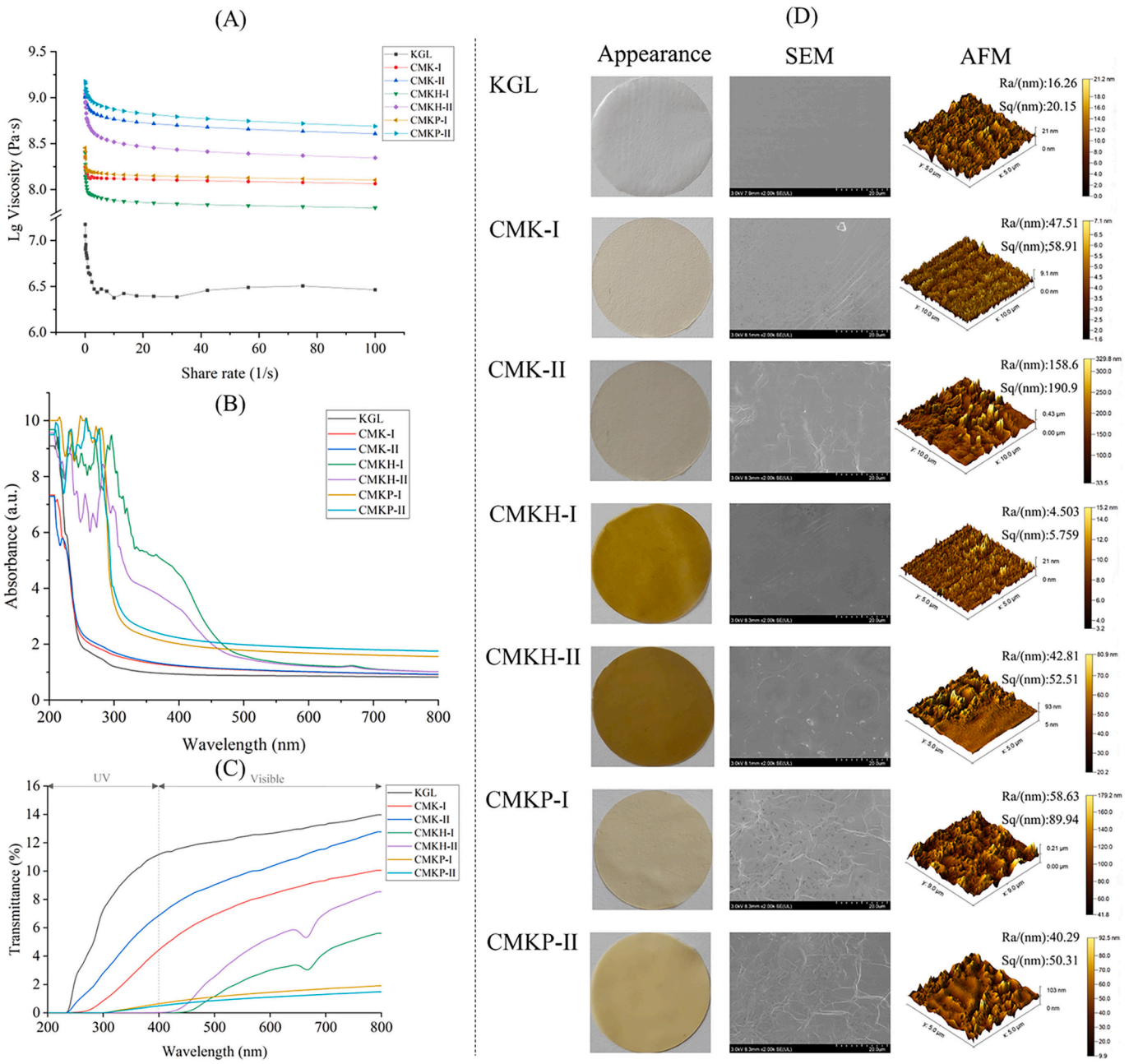

Fig. 1. (A) Viscosity as a function of shear rate of film solutions, (B) UV–Vis spectra (200–800 nm) of absorbance of edible films, (C) UV–Vis spectra (200–800 nm) of transmittance of edible films, (D) Surface appearance, scanning electron microscopy (SEM) and atomic force microscopy (AFM) analyses of edible films.

because the phenolic compounds in HLE formed a heterogeneous network structure with discontinuous regions and affected the structural integrity of the film (Vargas-Torrico et al., 2022). The addition of PS increases the EB and TS of CMKP films, which is possibly due to the increase in film thickness after addition of PS.

3.3. Film solubility and water vapor permeability (WVP)

As shown in Table 2, the weight loss (WL) of KGL reached 92.38% after 24 h. After adding CMKGM, the WL of the CMK-I/II films decreased, which possibly because the carboxymethylation modification increased its hydrophobicity and reduced its water absorption and solubility of KGM (Xiao et al., 2015). Compared to CMK films, the WL of the CMKH films increased, which possibly because the bioactive ingredients contained in HLE are water-soluble (Shivangi et al., 2021). After adding PS, the solubility of the film further improved, which may be due to the existence of water-soluble carboxylic acid groups in potassium sorbate (Xiao et al., 2015).

Good films should have a low WVP to prevent moisture migration and prolong food preservation time. The WVP of KGL was 3.50 g m^{-1} s^{-1} Pa^{-1}. The WVP value of film CMK-I/II decreased, indicating that the addition of CMKGM beneficial for improving the water blocking ability. After adding HLE, the WVP values of the CMKH-I and CMKH-II films were smaller than those of the CMK-I and CMK-II films, respectively. This might because the interaction between the HLE and the film matrix is not conducive to form intermolecular bonds between the biopolymer matrix and water molecules (Vargas-Torrico et al., 2022). However, the addition of PS (CMKP-I/II) increases the WVP value, thereby weakening the water barrier properties; thus, it is not conducive to food preservation. To sum up, the wvp value of the CMKH-I/II films are the lowest, indicating that adding HLE to the composite film can more effectively prevent water loss in food, so more conducive to food preservation.

Table 2
Characterisation values of different films.

	KGL	CMK-I	CMK-II	CMKH-I	CMKH-II	CMKP-I	CMKP-II
Total phenolic content (mg CAE/g film)	–	–	–	37.00 ± 0.13^{a}	38.68±±0.78^{a}	–	–
Thickness (mm)	0.062 ± 0.001^{d}	0.086 ± 0.007^{c}	0.097 ± 0.006^{b}	0.102 ± 0.005^{ab}	0.109 ± 0.005^{a}	0.105 ± 0.002^{ab}	0.112 ± 0.002^{a}
Tensile strength (MPa)	10.01 ± 1.39^{bc}	8.11 ± 0.60^{c}	13.02 ± 2.23^{ab}	8.805 ± 0.44^{c}	8.03 ± 1.61^{c}	10.75 ± 0.56^{abc}	13.13 ± 1.47^{a}
Elongation at break (%)	61.33 ± 6.02^{d}	81.33 ± 2.63^{b}	55.43 ± 2.42^{d}	113.15 ± 1.83^{a}	83.13 ± 4.16^{b}	77.05 ± 3.14^{bc}	71.73 ± 0.52^{c}
Weight loss (%)	92.38 ± 1.09^{c}	85.28 ± 0.17^{e}	82.24 ± 0.49^{f}	88.24 ± 0.81^{d}	88.27 ± 0.66^{d}	95.15 ± 0.34^{b}	96.91 ± 0.11^{a}
Water vapor permeability ($\times 10^{-10}$ g m^{-1} s^{-1} Pa^{-1})	3.50 ± 0.16^{a}	3.02 ± 0.02^{b}	2.89 ± 0.10^{b,c}	2.89 ± 0.04^{b,c}	2.64 ± 0.12^{c}	3.34 ± 0.07^{a}	3.34 ± 0.23^{a}
Opacity (Abs/mm)	13.64 ± 1.34^{b}	12.03 ± 0.44^{bc}	10.84 ± 0.82^{c}	12.75 ± 0.73^{b}	11.06 ± 0.14^{c}	17.10 ± 0.80^{a}	16.86 ± 0.138^{a}
L^*	90.72 ± 0.49^{a}	89.75 ± 0.37^{b}	88.84 ± 0.69^{b,c}	74.63 ± 0.56^{d}	74.36 ± 0.73^{d}	88.17 ± 0.62^{c}	87.83 ± 0.62^{c}
a^*	−1.47 ± 0.04^{d}	−1.04 ± 0.09^{c}	−0.98 ± 0.05^{c}	2.45 ± 0.30^{b}	2.76 ± 0.46^{a}	−1.09 ± 0.21^{c}	−0.98 ± 0.13^{c}
b^*	−0.17 ± 0.23^{e}	2.76 ± 0.94^{d}	3.88 ± 0.48^{d}	34.25 ± 0.46^{b}	36.29 ± 0.92^{a}	8.71 ± 1.34^{c}	9.95 ± 1.14^{c}
ΔE	1.54 ± 0.09^{e}	2.99 ± 0.84^{d,e}	4.01 ± 0.46^{d}	34.34 ± 0.48^{b}	36.41 ± 0.95^{a}	8.79 ± 1.31^{c}	10.00 ± 1.13^{c}

CAE, chlorogenic acid equivalent. The value is mean ± standard deviation (n = 3). Different letters in the same row indicate significant difference ($p < 0.05$).

3.4. Light blocking properties and opacity of the edible films

Ultraviolet light (200–280 nm) can accelerate the oxidation and decomposition of foods, which leads to food deterioration (Guo, Ge, Li, Mu, & Li, 2014). Therefore, food film must be protected from light to minimize oxidation. As shown in Fig. 1B, KGL film showed slight absorbance and transmittance because gelatin contains a large amount of aromatic amino acids and polypeptide bonds. The transmittance of the CMK-I/II film is lower than that of the KGL film, which suggested that CMKGM can enhance the UV–visible light blocking performance. The addition of HLE (CMKH-I/II) and PS (CMKP-I/II) can further improve the UV–visible light blocking capabilities. However, the absorption intensity of the CMKH film at approximately 200–350 nm was enhanced, and the transmittance in the UV region (200–400 nm) was close to zero (Fig. 1C), which indicates that the HLE composite films (CMKH-I/II) showed excellent shielding ability against UV light. This ability may be related to the existence of bioactive ingredients such as polyphenols, flavonoids, quinines, etc. (Chakravartula, Lourenço, Balestra, Bittante, Sobral, & Rosa, 2020).

The opacities at 600 nm of CMK-I and CMK-II were 11.70 and 10.45 (Abs/mm), respectively, which were lower than that of KGL. However, after adding HLE, the opacity of the edible films CMKH-I and CMKH-II increased to 12.37 and 11.89 (Abs/mm), respectively (Table 2). The opacity increase of the CMKH films is closely related to the film thickness and the substances in HLE. These results are consistent with those in other studies on gum-based films containing mulberry leaf extract (Shivangi et al., 2021). Overall, the composite films containing HLE showed excellent light blocking performance.

3.5. Chromatic aberration

As shown in Fig. 1D, the KGL film was transparent. After adding CMKGM, the film was slightly yellowish, and with increasing CMKGM content, the values of L^* (lightness) decreased, and the values of a^* (redness^{+}/greenness^{-}) and b^* (yellowness^{+}/blueness^{-}) increased (Table 2). The color of the CMKH-I and CMKH-II films was light brownish yellow, and with increasing HLE addition, the brown color deepened. The L^* value of CMKH-I/II is lower, and the a^* and b^* values are higher than those of the other films (Table 2). Currently, the edible films used commercially are mainly colorless. However, the bioactive edible film with plant extracts as the main raw material is usually colorful. This is mainly caused by the colored substances contained in the extracts such as anthocyanins and polyphenols (Vargas-Torrico et al., 2022). In fact, the greater color intensity of edible films showed a greater advantage for protecting against food deterioration by photo-oxidation reactions (Souza et al., 2017). Therefore, the application of colored edible films may be increasingly extensive in the future.

3.6. Surface morphology of the edible films

3.6.1. SEM

As shown in Fig. 1D, the KGL films were smooth, dense and uniform and were flat without bulges, exhibiting good compatibility between film-forming substrates. All the films showed more flexible and softer due to the indefinite structure of gelatin. The addition of CMKGM affects the surface of the film slightly unevenly. This possibly due to the electrostatic interaction between the carboxymethyl group in the CMKGM molecule and the amino group in the gelatin to form a network structure (Wang et al., 2022), and resulted in a compact morphology of the CMK film. With the addition of HLE, cracks and visible voids were observed in the films, and there were slight agglomerations, which confirmed that HLE affected the microstructure of the biopolymer network. This may be that the natural extract contains a large amount of phenolic compounds (Chakravartula et al., 2020). The combination of phenolic hydroxyl groups in HLE and KGM/CMKGM could decrease the polymerization degree of molecular chain and make the microstructure of the CMKH film denser (You, Wang, Zhou, Yang, & Pang, 2022), which is beneficial to enhance the water vapor barrier and mechanical properties of CMKH films. The addition of PS made the CMKP films exhibit a uniform and compact structure, but a few dark spots appeared in the structure of the CMKP-I/II films (Fig. 1D). These results seem likely to be due to encapsulated air microbubbles in the film matrix (Kowalczyk et al., 2020).

3.6.2. AFM

As shown in Fig. 1D, because of the good film-forming ability of KGM and gelatin, the surface of KGL film is relatively smooth and uniform, the mean roughness (Ra) and root mean square roughness (Rq) value was 16.26 and 20.15, respectively. The addition of CMKGM changes the surface structure of the film, increasing its surface roughness. When 2% CMKGM was added, the Ra and Rq of film CMK-I increased to 47.51 and 58.91, respectively, which became slightly rough; when CMKGM was added to 3%, the Ra and Rq of film CMK-II further increased to 158.6 and 190.9. However, the addition of HLE decreased the surface roughness of the CMKH film compared with CMK-I and CMK-II, probably because of the phenolic hydroxyl in the extract made the internal structure of the film denser, so decreases the surface roughness. What's more, the introduction of HLE might weaken the force strength between other groups, reduce the degree of molecular polymerization, and makes the surface of the film flatter. The observation results of AFM showed that the active compounds in HLE have good compatibility and uniform distribution in the membrane matrix, which is consistent with the results of SEM observation. The surface roughness of CMKP film increases with the addition of PS, which may be related to the high crystallinity of PS.

3.7. XRD

Both gelatin and KGM show broad peaks with amorphous structure characteristics at approximately 2θ = 20.00° (Meng et al., 2020), which may be due to the lack of space regularity of the molecular chains of the two compounds. The molecular arrangement is loose, and the crystal characteristics can be described as "long-range disorder, short-range order" (Zhang, Zhao, et al., 2022). As shown in Fig. 2A, KGL has a wide peak at 2θ (20.01°), indicating that the molecular interaction is very weak and the molecular arrangement is loose. CMK-I has a diffraction peak at 21.04°, but the diffraction peak of CMK-II is weaker than that of CMK-I (Fig. 2B&C), which is attributed to the destruction of the crystal structure of KGM by carboxymethylation (Zhang, Zhao, et al., 2022). However, after the addition of HLE, the peak at 21.14° was further strengthened (Fig. 2D&E), indicating that the addition of the complex components of HLE was beneficial to the enhancement of the degree of crystallization. CMKP-I/II showed a strong diffraction peak at approximately 4.60° and weak diffraction peaks at 13.99°, 17.35°, 21.37°, 28.22°, and 31.18° (Fig. 2F&G), which indicates that PS exists independently in the film as a strongly crystalline component.

3.8. FT-IR spectroscopy

As shown in Fig. 3A, the infrared spectrum of KGL film has a peak of O—H tensile vibration at 3292 cm^{-1}. After the addition of CMKGM, the peak shifted from 3292 cm^{-1} to 3275 cm^{-1} and became flat, which may be due to the presence of a carboxymethyl group forms new hydrogen bonds. The addition of HLE slightly shifted the O—H stretching vibration peak to the left (wavelength increased), and the peak amplitude became flat, which possibly because the interaction between phenolic acids in substances reduces the stretching of free hydroxyl groups (Lei et al., 2019). With the addition of PS, the –OH peak became flat, but the position was not shifted, which may be due to the hydrogen bonding between PS and the polymer resulting in the weakening of the –OH peak intensity (Kowalczyk et al., 2020).

For KGL, the peak of 1643 cm^{-1} is related to the carbonyl group and tensile vibrations, and the peak of 1554 cm^{-1} is caused by bending vibration of –NH in the polypeptide chain of the gelatin molecule (Kowalczyk et al., 2020). Films containing CMKGM have two additional peaks at approximately 1592 cm^{-1} and 1409 cm^{-1}, which are related to the symmetric and asymmetric stretching tensile vibrations of –COOH. Meanwhile, the peak at approximately 1592 cm^{-1} may also be related to the electrostatic attraction between –NH groups in gelatin and –COO– groups in CMKGM (Xiao, Wang, Xu, & Huang, 2019). Compared to KGL, the carbonyl absorption peaks of the CMK films at 1642 cm^{-1} were significantly weakened, which possibly because the relative proportion of KGM was reduced in the materials with the increasing of CMKGM content, and the peak was masked by the carboxymethyl (–COOH) group of CMKGM. When HLE was added to the composite films, more hydrogen bond interactions were introduced, and the interaction between other groups was reduced; thus, the peak shape was weakened. Specifically, the peaks of the –OH bond weakened more clearly. No other new peaks were examined in the CMKH blend film, suggesting that no new covalent connections were formed between the other film materials and the bioactive compound.

3.9. Thermal properties of the edible films

As shown in Fig. 3B&C, the degradation of the film can be divided into 3 stages. The first stage is mainly 70–160 °C (Fig. 3B), which is related to the evaporation of water, the breaking of intermolecular and intramolecular hydrogen bonds, and the loss of volatile compounds (Marangoni Júnior & Gonçalves, 2022). Compared to KGL, and the maximum degradation temperatures of CMK-I, CMK-II CMKH-I and CMKH-II increased to 119, 117, 109 and 123 °C, respectively (Fig. 3B), demonstrating that the introduce of HLE will affect the maximum degradation temperature of the first stage. The second stage is the most pronounced area of weight loss (Fig. 3C), which can be attributed to the degradation of the polymer backbone (Li et al., 2022). The maximum degradation temperature of KGL is 227 °C, and the mass loss is 63.90%. The mass loss was reduced to 50.92% and 45.18% for the CMK-I and CMK-II films, respectively, which indicated that the thermal stability of the film can be enhanced by introducing CMKGM. After adding HLE and PS, the mass losses of CMKH-I, CMKH-II, CMKP-I and CMKH-II further decreased to 50.08%, 48.51%, 37.77% and 39.90%, respectively (Fig. 3C), indicating that HLE and PS had a greater impact on the film thermal stability at this stage. The third stage located in the area at approximately 400 °C is mainly due to the weight loss caused by the

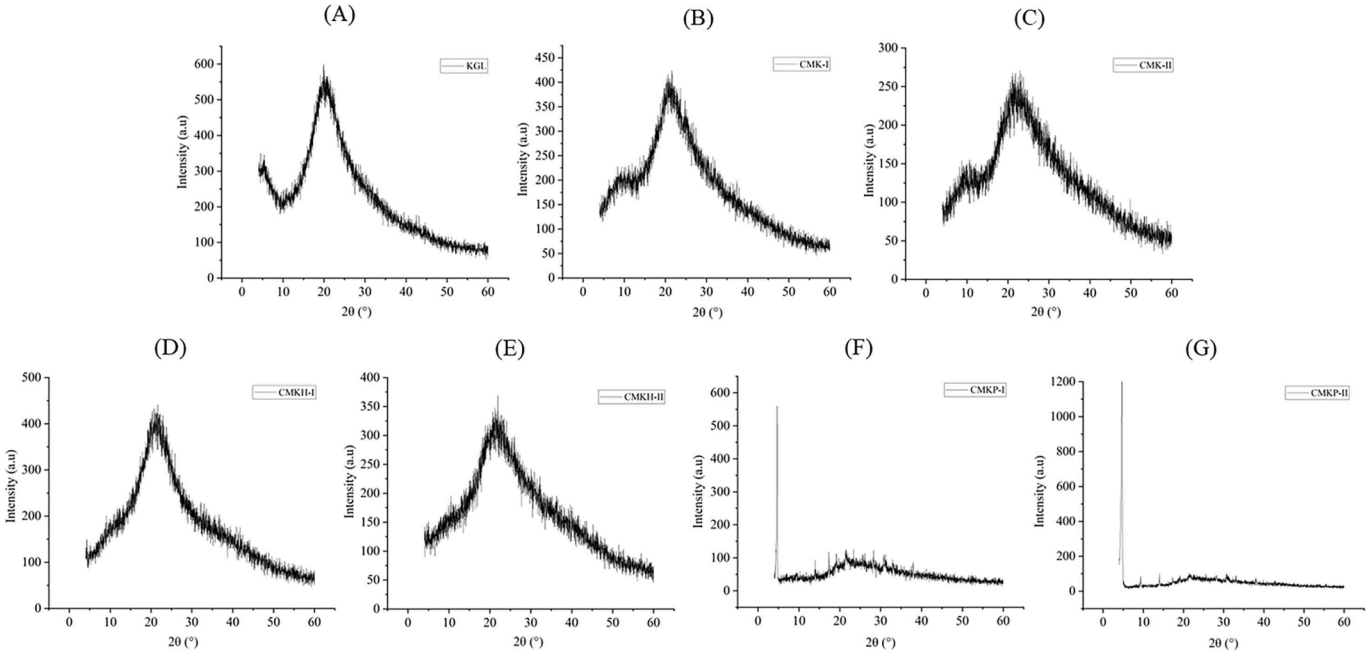

Fig. 2. X-ray diffraction (XRD) of different edible films. A: KGL, B: CMK-I, C: CMK-II, D: CMKH-I, E: CMKH-II, F: CMKP-I, G: CMKP-II.

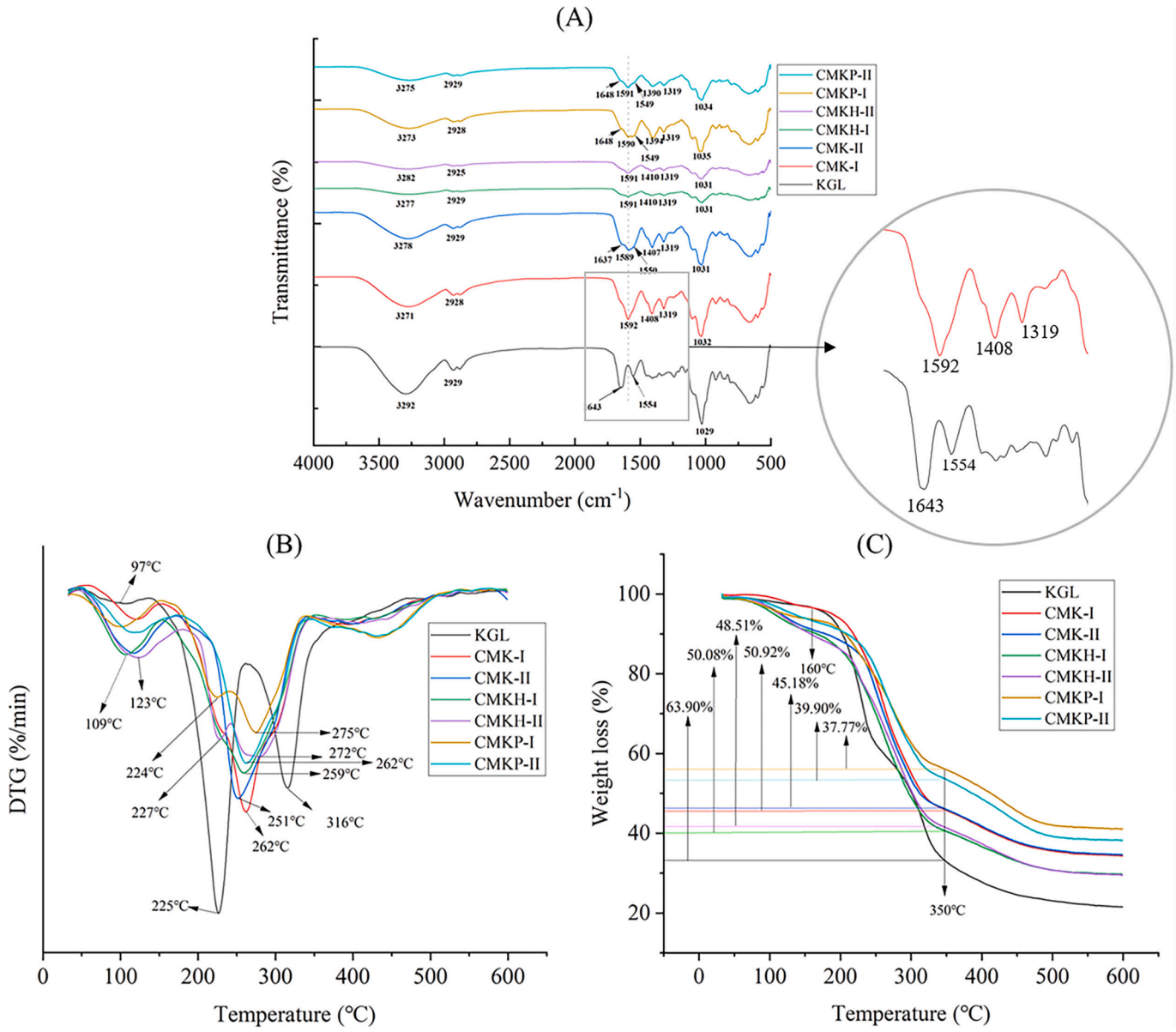

Fig. 3. Fourier transform infrared (FT-IR) spectra (A), derivative thermogravimetric curve (DTG) (B) and thermogravimetric curve (TG) (C) of different edible films.

Table 3
Antioxidant and antimicrobial activities of different films.

Films	Antioxidant activity		Antimicrobial activity					
	DPPH scavenging (%)	ABTS scavenging (%)	*S. aureus*		*L. monocytogenes*		*E.coli*	
			Diameter of inhibition (mm)	Inhibition rate (%)	Diameter of inhibition (mm)	Inhibition rate (%)	Diameter of inhibition (mm)	Inhibition rate (%)
Standards (Vc)	93.45 ± 0.007	93.69 ± 0.002	–	–	–	–	–	–
KGL	25.21 ± 0.010^{bc}	26.10 ± 0.005^{b}	–	–	–	–	–	–
CMK-I	24.93 ± 0.009^{bc}	24.90 ± 0.010^{bc}	–	–	–	–	–	–
CMK-II	24.07 ± 0.019^{c}	24.85 ± 0.014^{bc}	–	–	–	–	–	–
CMKH-I	83.76 ± 0.007^{a}	89.98 ± 0.004^{a}	20.98 ± 0.06^{a}	96.75 ± 0.27^{b}	20.08 ± 0.05^{b}	89.77 ± 3.08^{a}	21.18 ± 0.12^{c}	89.40 ± 1.43^{a}
CMKH-II	85.75 ± 0.014^{a}	90.93 ± 0.006^{a}	20.88 ± 0.21^{ab}	96.81 ± 0.43^{b}	20.95 ± 0.08^{a}	89.81 ± 2.62^{a}	20.82 ± 0.12^{d}	89.94 ± 1.86^{a}
CMKP-I	26.35 ± 0.019^{bc}	24.35 ± 0.012^{bc}	20.59 ± 0.20^{ab}	99.46 ± 0.34^{a}	19.93 ± 0.06^{b}	91.39 ± 1.2^{a}	22.07 ± 0.06^{a}	91.69 ± 1.17^{a}
CMKP-II	27.64 ± 0.009^{b}	23.65 ± 0.011^{c}	20.47 ± 0.18^{b}	99.15 ± 0.37^{a}	20.76 ± 0.13^{a}	90.14 ± 1.04^{a}	21.81 ± 0.04^{b}	91.08 ± 3.30^{a}

The value is mean ± standard deviation (n = 3). Different letters in the same column indicate significant difference ($p < 0.05$).

destruction of solid carbon structures containing polycyclic aromatic hydrocarbons (Shivangi et al., 2021).

3.10. Antioxidant activities of the edible films

According to Table 3. KGL, CMK-I and CMK-II films showed slightly scavenging ability, which can be attributed to the existence of hydroxyl groups and –NH groups in the molecular structure of gelatin, which act as electron donors in the films and can eliminate free radicals. The addition of PS did not significantly increase the antioxidant activities of films. However, HLE addition dramatically increased the antioxidant activities, and the DPPH and ABTS scavenging capacity ranged from 83% to 90%, which was close to the antioxidant capacity of Vc. The improvement in the antioxidant properties of the films may be closely related to the bioactive ingredients in HLE, such as polyphenols (Shivangi et al., 2021; Vargas-Torrico et al., 2022). Honeysuckle leaves are rich in various plant secondary metabolites, including phenolic acids, flavonoids, anthocyanins, tannins and so on. As a natural polyphenol, chlorogenic acid has excellent antioxidant and antibacterial activities, which can enhance the biological activity of the film. In this study, the total phenolic content in the CMKH films reached 37.00 and 38.68 mg CAE/g film, respectively (Table 1). The results suggested that the composite edible film containing HLE had excellent antioxidant properties.

3.11. Antibacterial activities of the edible films

Microbe are the commonest cause affecting food spoilage and human illness, so it is very important to develop effective antibacterial agents and bacteriostatic techniques for guarantee food safety (Luo et al., 2023). The antibacterial activity of CMKH films and CMKP films against *S. aureus* and *L. monocytogenes* (G^+) and *E. coli* (G^-) was evaluated by the disc diffusion method and viable cell inhibition rate method. As shown in Table 3 and Supplementary Fig. S1, no inhibitory effect was observed in the films of KGL, CMK-I, and CMK-II. Gelatin itself has no obvious antiseptic and bacteriostatic ability, but it helps to delay the degradation of protein (Feng, Bansal, & Yang, 2016). The addition of HLE showed good antibacterial activities. The inhibition rates of CMKH-I and CMKH-II films for the three indicator pathogens were close to or even higher than 90%, especially for *S. aureus*, which was the most sensitive strain. The PS composite film CMKP-I/II showed the highest inhibition rate against *S. aureus* because PS is a good food preservative with broad-spectrum antibacterial products. However, the inhibition rate and diameter of inhibition of HLE composite films CMKH-I/II showed similar antibacterial activity to *L. monocytogenes* and *E. coli* compared to CMKP films (Table 3). The excellent bacteriostasis of CMKH films may mainly be endowed by the phenolics and other active ingredients in the extracts. Phenolics can be used as broad-spectrum antibacterial products that can cause irreversible changes in the membrane properties of various microorganisms (Hossain et al., 2023). Phenolics (such as chlorogenic acid) can inhibit extracellular microbial enzymes and deprive the substrate needed for microbial growth, resulting in bubbles and depressions in the cell wall, resulting in the destruction of the integrity of the cell structure. Due to the damage to the cell wall, phenolics are easy to enter the cell plasma membrane, limiting the synthesis of nucleic acid, thus having bacteriostatic effect (Liu, Kai, & Yang, 2023). In this study, the total phenolic content (equivalent to chlorogenic acid) of the film was up to 38 mg/g dry films (Table 1); that is, in the culture system for the determination of the inhibition rate method, the phenolic content was approximately 0.76 mg/mL, which was higher than the minimum inhibitory concentration (MIC) of chlorogenic acid (Ozcelik, Kartal, & Orhan, 2011). Meanwhile, a previous study indicated that a mixture of multiple phenolics has better antibacterial effects than a single phenolic compound (Wen, Delaquis, Stanich, & Toivonen, 2003). The honeysuckle leaves are rich in a variety of phenolic compounds, which can jointly produce synergistic effects to inhibit the growth of pathogenic bacteria. These results indicated that composite films prepared with HLE have great potential application value in food preservation.

4. Conclusion

In this study, antioxidant and antibacterial edible films based on a CMKGM/KGM/gelatin matrix containing honeysuckle leaf extract (HLE) were prepared. The bioactive edible films have good water vapor barrier properties and thermal stability, and the introduction of HLE significantly enhanced the mechanical properties and light-blocking ability of the film. Structural characteristics analysis confirmed the compatibility of the film matrix and HLE, and the formation of a dense internal structure enhanced the physical properties of the film. The bioactive edible films showed good antioxidant and antibacterial activities; in particular, the bacteriostatic activities against *E. coli*, *L. monocytogenes*, and *S. aureus* were close to that of PS. Generally, this study suggested that CMKGM/KGM/gelatin combinations could be applied as a promising film-forming matrix, and most importantly, HLE, a low-value byproduct of the food industry, also has great potential to prepare bioactive edible films.

CRediT authorship contribution statement

Meng Wang: Data curation, Writing – original draft. **Yun-Cheng Li:** Methodology, Writing – original draft, Visualization. **Fan-Bing Meng:** Conceptualization, Writing – review & editing, Formal analysis. **Qiao Wang:** Writing – review & editing, Data curation. **Zheng-Wu Wang:** Resources, Funding acquisition. **Da-Yu Liu:** Project administration, Supervision.

Declaration of Competing Interest

The authors declare that they have no known competing financial interests or personal relationships that could have appeared to influence the work reported in this paper.

Data availability

No data was used for the research described in the article.

Acknowledgment

This work was supported by Sichuan Science and Technology Program (2022YFN0014, 2022YFN0052, 2021YFSY0034).

Appendix A. Supplementary data

Supplementary data to this article can be found online at https://doi.org/10.1016/j.fochx.2023.100675.

References

Biao, Y., Cao, Y., Tang, Q., Yuan, Z., Zhou, Y., McClements, D. J., & Cao, C. (2019). Enhanced performance and functionality of active edible films by incorporating tea polyphenols into thin calcium alginate hydrogels. *Food Hydrocolloids, 97*, Article 105197. https://doi.org/10.1016/j.foodhyd.2019.105197

Carneiro-da-Cunha, M. G., Cerqueira, M. A., Souza, B. W. S., Teixeira, J. A., & Vicente, A. A. (2011). Influence of concentration, ionic strength and pH on zeta potential and mean hydrodynamic diameter of edible polysaccharide solutions envisaged for multinanolayered films production. *Carbohydrate Polymers, 85*(3), 522–528. https://doi.org/10.1016/j.carbpol.2011.03.001

Chakravartula, S. S. N., Lourenço, R. V., Balestra, F., Bittante, A. M. Q. B., Sobral, P. J. d. A., & Rosa, M. D. (2020). Influence of pitanga (*Eugenia uniflora* L.) leaf extract and/or natamycin on properties of cassava starch/chitosan active films. *Food Packaging and Shelf Life, 24*, 100498.

Feng, X., Bansal, N., & Yang, S. (2016). Fish gelatin combined with chitosan coating inhibits myofibril degradation of golden pomfret (*Trachinotus blochii*) fillet during cold storage. *Food Chemistry, 200*, 283–292. https://doi.org/10.1016/j.foodchem.2016.01.030

Fidelis, J. C. F., Marchi, L. B., Scapim, M. R. S., Gobetti, N. D., Yamashita, F., & Monteiro, A. R. G. (2022). Development of biodegradable films containing

pomegranate peel extract and potassium sorbate. *LWT, 160*, Article 113302. https://doi.org/10.1016/j.lwt.2022.113302

Guo, J., Ge, L., Li, X., Mu, C., & Li, D. (2014). Periodate oxidation of xanthan gum and its crosslinking effects on gelatin-based edible films. *Food Hydrocolloids, 39*, 243–250. https://doi.org/10.1016/j.foodhyd.2014.01.026

He, B., Wang, Y., Jiang, Z., Liu, S., & Zhu, J. (2021). Physical properties and antibacterial activity of the composited films based on carboxymethyl cellulose and gelatin functionalized with epsilon-polylysine. *International Journal of Biological Macromolecules, 191*, 1126–1136. https://doi.org/10.1016/j.ijbiomac.2021.09.181

Hossain, M. S., Shahiduzzaman, M., Rahim, M. A., Paul, M., Sarkar, R., Chaity, F. S., … Islam, S. (2023). Bioactive properties and organosulfur compounds profiling of newly developed garlic varieties of Bangladesh. *Food Chemistry: X, 17*, Article 100577. https://doi.org/10.1016/j.fochx.2023.100577

Kowalczyk, D., Kordowska-Wiater, M., Karaś, M., Zięba, E., Mężyńska, M., & Wiącek, A. E. (2020). Release kinetics and antimicrobial properties of the potassium sorbate-loaded edible films made from pullulan, gelatin and their blends. *Food Hydrocolloids, 101*, Article 105539. https://doi.org/10.1016/j.foodhyd.2019.105539

Lei, Y., Wu, H., Jiao, C., Jiang, Y., Liu, R., Xiao, D., … Li, S. (2019). Investigation of the structural and physical properties, antioxidant and antimicrobial activity of pectin-konjac glucomannan composite edible films incorporated with tea polyphenol. *Food Hydrocolloids, 94*, 128–135. https://doi.org/10.1016/j.foodhyd.2019.03.011

Li, Y. C., Du, W., Meng, F. B., Rao, J. W., Liu, D. Y., & Peng, L. X. (2021). Tartary buckwheat protein hydrolysates enhance the salt tolerance of the soy sauce fermentation yeast *Zygosaccharomyces rouxii*. *Food Chemistry, 342*, Article 128382. https://doi.org/10.1016/j.foodchem.2020.128382

Li, R.-J., Kuang, X.-P., Wang, W.-J., Wan, C.-P., & Li, W.-X. (2020). Comparison of chemical constitution and bioactivity among different parts of Lonicera japonica Thunb. *Journal of the Science of Food and Agriculture, 100*(2), 614–622. https://doi.org/10.1002/jsfa.10056

Li, Y.-C., Luo, Y., Meng, F.-B., Li, J., Chen, W.-J., Liu, D.-Y., … Zhou, L. (2022). Preparation and characterization of feruloylated oat β-glucan with antioxidant activity and colon-targeted delivery. *Carbohydrate Polymers, 279*, Article 119002. https://doi.org/10.1016/j.carbpol.2021.119002

Liu, Y., Kai, Y., & Yang, H.-S. (2023). Biodegradable fish gelatin/chitosan-based active films alter chill-stored golden pomfret (*Trachinotus blochii*) metabolites mainly through modulating four metabolic pathways. *Food Packaging and Shelf Life, 36*, Article 101046. https://doi.org/10.1016/j.fpsl.2023.101046

Liu, Z., Lin, D., Lopez-Sanchez, P., & Yang, X. (2020). Characterizations of bacterial cellulose nanofibers reinforced edible films based on konjac glucomannan. *International Journal of Biological Macromolecules, 145*, 634–645. https://doi.org/10.1016/j.ijbiomac.2019.12.109

Luo, Y., Li, Y.-C., Meng, F.-B., Wang, Z.-W., Liu, D.-Y., Chen, W.-J., & Zou, L.-H. (2023). Simultaneously enhanced stability and biological activities of chlorogenic acid by covalent grafting with soluble oat β-glucan. *Food Chemistry: X, 17*, Article 100546. https://doi.org/10.1016/j.fochx.2022.100546

Marangoni Júnior, L., Gonçalves, S. d. Á., Silva, R. G. d., Martins, J. T., Vicente, A. A., Alves, R. M. V., & Vieira, R. P. (2022). Effect of green propolis extract on functional properties of active pectin-based films. *Food Hydrocolloids, 131*, 107746. doi: 10.1016/j.foodhyd.2022.107746.

Meng, F.-B., Gou, Z.-Z., Li, Y.-C., Zou, L.-H., Chen, W.-J., & Liu, D.-Y. (2022). The efficiency of lemon essential oil-based nanoemulsions on the inhibition of *Phomopsis* sp. and reduction of postharvest decay of kiwifruit. *Foods, 11*(10), 1510. https://www.mdpi.com/2304-8158/11/10/1510.

Meng, F. B., Lei, Y. T., Zhang, Q., Li, Y. C., Chen, W. J., & Liu, D. Y. (2022). Encapsulation of *Zanthoxylum bungeanum* essential oil to enhance flavor stability and inhibit lipid oxidation of Chinese-style sausage. *Journal of the Science of Food and Agriculture, 102*(10), 4035–4045. https://doi.org/10.1002/jsfa.11752

Meng, F. B., Zhang, Q., Li, Y. C., Li, J. J., Liu, D. Y., & Peng, L. X. (2020). Konjac glucomannan octenyl succinate as a novel encapsulation wall material to improve curcumin stability and bioavailability. *Carbohydrate Polymers, 238*, Article 116193. https://doi.org/10.1016/j.carbpol.2020.116193

Meng, F.-B., Zhou, L., Li, J.-J., Li, Y.-C., Wang, M., Zou, L.-H., … Chen, W.-J. (2022). The combined effect of protein hydrolysis and Lactobacillus plantarum fermentation on antioxidant activity and metabolomic profiles of quinoa beverage. *Food Research International, 157*, Article 111416. https://doi.org/10.1016/j.foodres.2022.111416

Ozcelik, B., Kartal, M., & Orhan, I. (2011). Cytotoxicity, antiviral and antimicrobial activities of alkaloids, flavonoids, and phenolic acids. *Pharmaceutical Biology, 49*(4), 396–402. https://doi.org/10.3109/13880209.2010.519390

Ran, X.-L., Lou, X.-W., Zheng, H.-Q., Gu, Q.-Y., & Yang, H.-S. (2022). Improving the texture and rheological qualities of a plant-based fishball analogue by using konjac glucomannan to enhance crosslinks with soy protein. *Innovative Food Science and Emerging Technologies, 75*, Article 102910. https://doi.org/10.1016/j.ifset.2021.102910

Rao, J.-W., Meng, F.-B., Li, Y.-C., Chen, W.-J., Liu, D.-Y., & Zhang, J.-M. (2022). Effect of cooking methods on the edible, nutritive qualities and volatile flavor compounds of rabbit meat. *Journal of the Science of Food and Agriculture, 102*(10), 4218–4228. https://doi.org/10.1002/jsfa.11773

Rather, J. A., Akhter, N., Ashraf, Q. S., Mir, S. A., Makroo, H. A., Majid, D., Barba, F. J., Khaneghah, A. M., & Dar, B. N. (2022). A comprehensive review on gelatin: Understanding impact of the sources, extraction methods, and modifications on potential packaging applications. *Food Packaging and Shelf Life, 34*, Article 100945. https://doi.org/10.1016/j.fpsl.2022.100945

Sáez-Orviz, S., Marcet, I., Rendueles, M., & Díaz, M. (2021). Bioactive packaging based on delipidated egg yolk protein edible films with lactobionic acid and *Lactobacillus plantarum* CECT 9567: Characterization and use as coating in a food model. *Food Hydrocolloids, 119*, Article 106849. https://doi.org/10.1016/j.foodhyd.2021.106849

Semwal, A., Ambatipudi, K., & Navani, N. K. (2022). Development and characterization of sodium caseinate based probiotic edible film with chia mucilage as a protectant for the safe delivery of probiotics in functional bakery. *Food Hydrocolloids for Health, 2*, Article 100065. https://doi.org/10.1016/j.fhfh.2022.100065

Shang, X., Pan, H., Li, M., Miao, X., & Ding, H. (2011). *Lonicera japonica* Thunb.: Ethnopharmacology, phytochemistry and pharmacology of an important traditional Chinese medicine. *Journal of Ethnopharmacology, 138*(1), 1–21. https://doi.org/10.1016/j.jep.2011.08.016

Shivangi, S., Dorairaj, D., Negi, P. S., & Shetty, N. P. (2021). Development and characterisation of a pectin-based edible film that contains mulberry leaf extract and its bio-active components. *Food Hydrocolloids, 121*, Article 107046. https://doi.org/10.1016/j.foodhyd.2021.107046

Souza, V. G. L., Fernando, A. L., Pires, J. R. A., Rodrigues, P. F., Lopes, A. A. S., & Fernandes, F. M. B. (2017). Physical properties of chitosan films incorporated with natural antioxidants. *Industrial Crops and Products, 107*, 565–572. https://doi.org/10.1016/j.indcrop.2017.04.056

Vargas-Torrico, M. F., von Borries-Medrano, E., & Aguilar-Mendez, M. A. (2022). Development of gelatin/carboxymethylcellulose active films containing Hass avocado peel extract and their application as a packaging for the preservation of berries. *International Journal of Biological Macromolecules, 206*, 1012–1025. https://doi.org/10.1016/j.ijbiomac.2022.03.101

Wang, L., Zhou, N., Zheng, S., & Pang, J. (2022). Formation of composite hydrogel of carboxymethyl konjac glucomannan/gelatin for sustained release of EGCG. *Food Science and Human Wellness, 11*(5), 1373–1383. https://doi.org/10.1016/j.fshw.2022.04.037

Wen, A., Delaquis, P., Stanich, K., & Toivonen, P. (2003). Antilisterial activity of selected phenolic acids. *Food Microbiology, 20*(3), 305–311. https://doi.org/10.1016/S0740-0020(02)00135-1

Xiao, M., Dai, S., Wang, L., Ni, X., Yan, W., Fang, Y., … Jiang, F. (2015). Carboxymethyl modification of konjac glucomannan affects water binding properties. *Carbohydrate Polymers, 130*, 1–8. https://doi.org/10.1016/j.carbpol.2015.05.001

Xiao, J.-X., Wang, L.-H., Xu, T.-C., & Huang, G.-Q. (2019). Complex coacervation of carboxymethyl konjac glucomannan and chitosan and coacervate characterization. *International Journal of Biological Macromolecules, 123*, 436–445. https://doi.org/10.1016/j.ijbiomac.2018.11.086

Xue, F., Gu, Y., Wang, Y., Li, C., & Adhikari, B. (2019). Encapsulation of essential oil in emulsion based edible films prepared by soy protein isolate-gum acacia conjugates. *Food Hydrocolloids, 96*, 178–189. https://doi.org/10.1016/j.foodhyd.2019.05.014

You, P., Wang, L., Zhou, N., Yang, Y., & Pang, J. (2022). A pH-intelligent response fish packaging film: Konjac glucomannan/carboxymethyl cellulose/blackcurrant anthocyanin antibacterial composite film. *International Journal of Biological Macromolecules, 204*, 386–396. https://doi.org/10.1016/j.ijbiomac.2022.02.027

Zhang, M., Ma, M., Yang, T., Li, M., & Sun, Q. (2022). Dynamic distribution and transition of gluten proteins during noodle processing. *Food Hydrocolloids, 123*, Article 107114. https://doi.org/10.1016/j.foodhyd.2021.107114

Zhang, Y., Zhao, Y., Yang, W., Song, G., Zhong, P., Ren, Y., & Zhong, G. (2022). Structural complexity of Konjac glucomannan and its derivatives governs the diversity and outputs of gut microbiota. *Carbohydrate Polymers, 292*, Article 119639. https://doi.org/10.1016/j.carbpol.2022.119639

Zhang, J., Zhu, L., Li, K., Ye, J., Xiao, X., Xue, M., … Chen, Y. (2022). Preparation of bio-based modified starch film and analysis of preservation mechanism for sweet cherry. *Food Chemistry: X, 16*, Article 100490. https://doi.org/10.1016/j.fochx.2022.100490